IEEE Robotics and Automation Letters (RA-L) paper, presented at ICRA 2026, Vienna, Austria. Cite as RA-L paper.

Robotic Harvesting of Delicate Fruit: Design and Implementation of an Under-Actuated Disturbance-Resistant Gripper

Jianguo Wang, *Graduate Student Member, IEEE*, Jihao Li, *Graduate Student Member, IEEE*, Jituo Li, *Member, IEEE*, Xiaoqiang Du, *Member, IEEE*, and Huixu Dong, *Member, IEEE*

***Abstract*—Agricultural harvesting grippers have emerged as a pivotal technology in the evolution of smart agriculture, enhancing efficient fruit collection. Existing grippers frequently fail to accommodate the diverse morphologies of fruits. Moreover, achieving stable grasping under external disturbances, such as natural wind, remains a significant challenge. To mitigate these limitations, we present a novel under-actuated gripper for fruit harvesting, alongside the formulation of innovative harvesting strategies aimed at optimizing both the harvest success rate and fruit integrity. Firstly, a strategy is developed to promote the success rate of harvesting operations under disturbance. The harvesting strategy involves stabilizing the fruit by enclosing the stem, followed by grasping and severing the stem to detach the fruit. Secondly, we propose an auxiliary locking and grasping coupling mechanism, which employs a single actuator to drive all gripper components, thereby reducing both cost and control complexity. Thirdly, a force distribution constraint unit is incorporated to allocate the actuator's power between grasping and shearing actions, enabling regulation of the grasping force to protect the fruit. Finally, the performance of the gripper is assessed through a series of rigorous experiments on fruits with diverse sizes, textures, and surface characteristics, demonstrating its superior efficacy in preserving fruit integrity during real-world harvesting scenarios.**

***Index Terms*—Harvesting robotics, under-actuated gripper, mechanical design, agricultural automation.**

Received 19 June 2025; accepted 20 October 2025. Date of publication 10 November 2025; date of current version 19 November 2025. This article was recommended for publication by Associate Editor C. Piazza and Editor C. Gosselin upon evaluation of the reviewers' comments. This work was supported in part by Zhejiang Provincial Natural Science Foundation of China under Grant No. LD24E050006 and the "Pioneer" and "Leading Goose" R&D Programs of Zhejiang Province under Grant No. 2025C01072, in part by the Research Program of Ningbo Science and Technology Bureau under Grant No. 2023Z128 and Grant No. 2025Z001, and in part by the National Natural Science Foundation of China Youth Program under Grant No. 52305037. *(Jianguo Wang and Jihao Li contributed equally to this work.) (Corresponding author: Huixu Dong.)*

Jianguo Wang, Jihao Li, and Huixu Dong are with the Grasp Lab, School of Mechanical Engineering, Zhejiang University, Hangzhou 310027, China, and also with Robotics Institute, Zhejiang University, Hangzhou 310027, China (e-mail: huixudong@zju.edu.cn).

Jituo Li is with Robotics Institute, Zhejiang University, Hangzhou 310027, China.

Xiaoqiang Du is with the Department of Mechanical Engineering, Zhejiang Sci-Tech University, Hangzhou 310018, China, and also with the Zhejiang Provincial Key Laboratory of Agricultural Intelligent Sensing and Robotics, Hangzhou 310018, China.

This article has supplementary downloadable material available at https://doi.org/10.1109/LRA.2025.3631358, provided by the authors.

Digital Object Identifier 10.1109/LRA.2025.3631358

I. Introduction

As GLOBAL food demand continues to escalate, agricultural robots are increasingly vital in automation and intelligent solutions for farmland inspection [1], pesticide spraying [2], and plant detection [3]. Among these advancements, harvesting robots represent a crucial sector specifically designed for the collection of fruits. The grasping ability of the robot hand provides technical support for fruit harvesting [4], [5], [6]. These robots not only mitigate labor intensity but also significantly enhance the speed and efficiency of the harvesting process, thereby ensuring both its effectiveness and quality [7], [8].

Fruit harvesting techniques employed by robotic systems can be broadly categorized into two primary methods: flexible separation and rigid separation [9]. Flexible separation primarily employs twisting, folding, and pulling techniques, making it suitable for fruits such as blackberries [10], kiwifruit [11], and cherry tomatoes [12], [13], where the bonding force between the fruit and stem is relatively weak. The flexible separation gripper integrates a soft adaptive mechanism to ensure gentle yet efficient harvesting. For instance, Gunderman et al. introduced a tendon-driven soft robotic gripper featuring active contact force feedback control for harvesting [10]. Similarly, Gao et al. designed a pneumatic gripper integrating clamping and rotation to facilitate fruit collection [12]. These grippers harvest the fruit by directly breaking off the stem, which requires that the stem of the fruit can be easily detached. Otherwise, excessive grasping force during this process can cause surface damage and compromise the structural integrity of the fruit. The stem-based perception harvest method [14] reduces damage but demands high visual system precision.

In contrast, rigid separation techniques are more adept at preserving the structural integrity of fruits, making them especially suitable for harvesting fruits with sturdier stems or delicate skins. For example, Xiong et al. [15] developed a cable-driven gripper with six fingers, forming an enclosed grasping space, integrated with a curved blade for cutting, specifically designed for efficient strawberry harvesting. However, this design is constrained by the requirement that the fruit must possess a long stalk and hang downward, thus limiting its versatility for harvesting fruits in other orientations. Additionally, some grippers combine suction cups with supplementary harvesting mechanisms, employing vacuum pressure to handle fruits such as tomatoes [16]. These

IEEE Robotics and Automation Letters (RA-L) paper, presented at ICRA 2026, Vienna, Austria. Cite as RA-L paper.

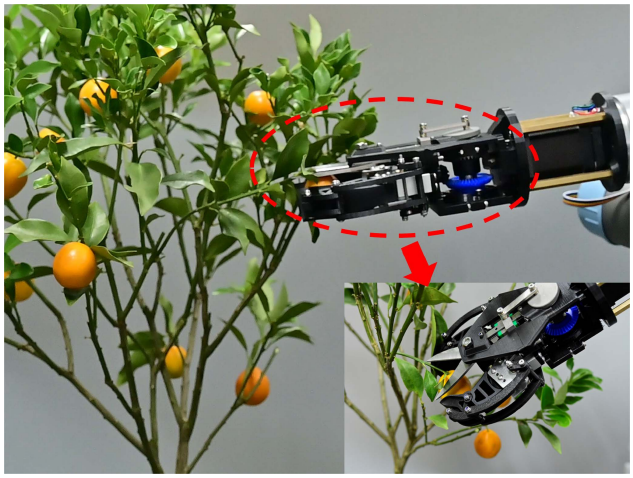

Fig. 1. Anti-disturbance gripper harvesting operation.

grippers are only proficient with fruits that have smooth surfaces, while they are ineffective on those with irregular textures. To address these challenges, certain grippers have been engineered as multifunctional modules, capable of executing the entire harvesting process, encompassing grasping, cutting, and placement. For example, Xu et al. [17] developed a navel orange harvesting gripper that integrates adsorption, clamping, and rotary cutting mechanisms into a unified system. Similarly, Yu et al. [18] introduced a citrus harvesting gripper incorporating both active and passive components. Nevertheless, these grippers depend on multiple motors, leading to increased structural complexity and greater control challenges.

The performance of the gripper is a crucial factor in the success of fruit harvesting. Considering the delicate nature of fruit and vegetable harvesting, the positioning accuracy of the robotic arm is essential to prevent damage and ensure efficient and precise picking [19], [20]. To enhance accuracy, robotic arms are often equipped with various sensors, including vision, tactile, and radar systems, which improve the success rate of harvesting [21], [22], [23]. However, these systems are complex and heavily reliant on sensor data and precise positioning. Moreover, external environmental disturbances such as wind during outdoor harvesting make it challenging to accurately track and locate the fruit.

In summary, the majority of existing grippers are constrained to harvesting specific fruit types, such as those with smooth surfaces or hard skins. This inherent limitation impairs their versatility for broader applications. These grippers often prove ineffective when attempting to harvest fruits with hard stems without causing damage to the fruit. Furthermore, these grippers require precise positioning and demonstrate limited resilience to external disturbances. Accordingly, the objective is to develop a fruit-harvesting gripper that is adaptable, capable of damage-free harvesting, and exhibits robust anti-disturbance capabilities.

To achieve these objectives, we propose a single motor driven gripper utilizing rigid separation method for efficient fruit harvesting, as depicted in Fig. 1. Firstly, we propose an innovative harvesting strategy where the gripper employs a shearing mechanism to secure the fruit stem, subsequently performing a series of actions including grasping, cutting, and placement. The shearing mechanism of the gripper has a broad opening range, allowing for the harvesting of the entire fruit upon the stem is inserted into the mechanism. Consequently, even if the positioning of the gripper is not precise or the fruit is displaced by external factors, the fruit can still be harvested. Notably, the shears do not sever the stem when securing the fruit, but only restrict its movement. Secondly, we divide the proposed gripper into three modules, including the grasping module, the shearing module as well as the auxiliary locking and grasping coupling mechanism. The fingers of the grasping module are constructed from soft materials, incorporating a curved inner surface and torsion springs at the joints. This design allows the fingers to conform more effectively to the shape of the fruit and form a cage-like enclosure around the fruit, thus improving grasp stability [24]. When combined with the shearing module, the mechanism enables the gripper to accommodate a diverse array of fruits with varying textures, weights, and surface characteristics. Thirdly, we incorporate a differential mechanism into the auxiliary locking and grasping coupling mechanism to allocate the output of a single motor between the shearing and grasping modules. It is noteworthy that a force distribution constraint unit is assembled at the grasping output terminal of the auxiliary locking and grasping coupling mechanism, allowing regulation of output distribution between the two modules. This enables us to establish distinct upper limits for grasping force in accordance with the firmness of the fruit, thereby preventing the fingers from exerting excessive pressure that could result in damage. Ultimately, we evaluate the grasping force in order to ascertain the efficacy of the power output distribution. Additionally, a series of experiments is conducted to validate the efficacy and versatility of the gripper in achieving damage-free harvesting, as well as to assess the gripper's robustness in harvesting trials under disturbed conditions.

We highlight that the primary contribution of our work is the development of an under-actuated fruit harvesting gripper characterized by disturbance rejection and adaptability. The first novelty is that we propose a harvesting strategy, which enhances the gripper's resilience against external disturbances and relieves its reliance on precise positioning through the implementation of an auxiliary fixation method. The second contribution features an auxiliary locking and grasping coupling mechanism. Based on the mechanical differential principle, the cutting and grasping components are driven by a single motor, which simplifies control method and reduces overall system cost. The force distribution constraint unit allocates the actuator's power between grasping and cutting actions, enabling the regulation of the grasping force to protect the fruit. This feature represents the third novelty.

The remainder of this letter is organized as follows: Section II presents the harvesting strategy, theoretical modeling, and mechanical design of the gripper. Section III describes the validation of the strategy and the performance experiments. Section IV provides an analysis and discussion of the experimental results. Finally, Section V concludes the letter.

II. Methodology

An anti-disturbance gripper is engineered for harvesting applications, particularly tailored to small fruits, integrating a novel

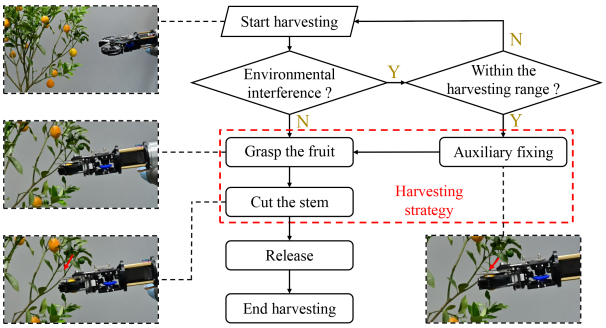

Fig. 2. Harvesting strategy flowchart.

harvesting strategy designed based on the idea of mutual cooperation between components to mitigate the effects of robotic arm positioning inaccuracies and environmental disturbances, thereby improving precision and operational efficiency. To enhance adaptability across a range of harvesting tasks, the gripper is outfitted with an efficient shearing mechanism and an adaptive grasping system. Driven by a single motor, the gripper minimizes actuator requirements, streamlines the control architecture, and reduces operational costs.

A. A Novel Harvesting Strategy

A widely adopted fruit harvesting strategy entails initially securing the fruit with a gripper, and subsequently detaching it using scissors. However, under conditions of fruit oscillation or imprecise positioning of the robotic arm, achieving a stable grasping with the gripper becomes notably difficult. In this section, a novel harvesting strategy, depicted in Fig. 2, has been devised: before grasping the fruit, the shearing mechanism closes around the fruit stem without severing it, effectively securing the fruit in place for stabilization. This stabilization enables the gripper fingers to grasp the fruit more steadily. Once the fruit is firmly grasped, the scissors continue to close, severing the stem to detach the fruit from the stalk. The target fruit typically has a large diameter, and the limited opening angle of the gripper makes effective direct grasping difficult. By contrast, the scissors provide a wider opening and only need to encompass the slender stem, which renders the task of stabilizing the stem considerably simpler. Consequently, when fruit localization is imprecise, the shearing mechanism tends to offer a more reliable means of fruit stabilization.

B. Design of the Linkage-Driven Shearing Mechanism

In comparison to direct grasping mechanisms, shearing-based harvesting systems provide enhanced versatility, especially for fruits with strong stem attachments. A linkage-driven shearing mechanism is engineered, as illustrated in Fig. 3(a-1). The rotation of the cam drives the slider to move linearly along the guide rail through link 1 (l_1), inducing the blades to open and close via the oscillation of link 2 (l_4). The motion sequence is illustrated in Fig. 3(a-2): as the slider advances toward the scissors, the blades open, and as it retracts, the blades close. A significant advantage of this mechanism lies in the controlled

TABLE I
SHEARING MECHANISM PARAMETER DESIGN

Parameter	r	l_0	l_1	l_2	l_3	l_4	l_5
Value (mm)	6	85	36	8	6	20	28

motion range of its scissors, particularly when compared to rotary cutters. This design feature effectively reduces the risk of damage from potential collisions. The torque analysis of the shearing mechanism is conducted to examine the relationship between the input torque of the driving cam and the output torque of the blades. Based on the geometric relationships shown in Fig. 3(a-3), the following length equations are derived:

$$l_0 = r\cos\theta_1 + l_1\cos\gamma + l_2 + l_4\cos\beta + l_5\cos\theta_2 \tag{1}$$

$$l_3 + l_4\sin\beta = l_5\sin\theta_2 \tag{2}$$

$$r\sin\theta_1 = l_1\sin\gamma \tag{3}$$

According to the principle of virtual work, for a small rotation increment:

$$T_i d\theta_1 = T_o d\theta_2 \tag{4}$$

$$\frac{T_o}{T_i} = \frac{d\theta_1}{d\theta_2} \tag{5}$$

Differentiating Eq. (1), (2), and (3):

$$r\sin\theta_1\,\mathrm{d}\theta_1 + l_1\sin\gamma\,\mathrm{d}\gamma + l_4\sin\beta\,\mathrm{d}\beta + l_5\sin\theta_2\,\mathrm{d}\theta_2 = 0 \tag{6}$$

$$l_4\cos\beta\,\mathrm{d}\beta = l_5\cos\theta_2\,\mathrm{d}\theta_2 \tag{7}$$

$$r\cos\theta_1\,\mathrm{d}\theta_1 = l_1\cos\gamma\,\mathrm{d}\gamma \tag{8}$$

Substituting the equations into Eq. (5) and rearranging:

$$\mu = \frac{T_o}{T_i} = \frac{d\theta_1}{d\theta_2} = -\frac{l_5\cos\gamma\sin(\theta_2+\beta)}{r\cos\beta\sin(\theta_1+\gamma)} \tag{9}$$

where, μ represents transmission ratio, γ and β are given by Eq. (2) and (3). The torque output is expressed as:

$$T_o = F_a l_6 \tag{10}$$

To mitigate sliding friction on the rod l_2, a guide rail system is adopted. Specifically, the slider (MGN7C, 22.5 × 17 × 6.5 mm) and its corresponding rail (7 × 4.8 mm) are selected to ensure dimensional compatibility. A standardized blade (88 × 18 × 3 mm) is employed as a replaceable consumable component. The parameter configuration is determined accordingly, with detailed specifications provided in Table I. The minimum transmission ratio of θ_1 from 0 to 2π is 4.19. For citrus fruits with hard stems, the scissors require a relatively large cutting force. With the leverage of the shearing mechanism, the motor provides sufficient torque to ensure effective cutting.

C. Design of Flexible Grasping Mechanism

As shown in Fig. 3(b-1), the grasping mechanism adopts an underactuated design to accommodate fruits of varying shapes. Each finger comprises a proximal and a distal phalanx, connected by a rotational pair with a torsion spring for

IEEE Robotics and Automation Letters (RA-L) paper, presented at ICRA 2026, Vienna, Austria. Cite as RA-L paper.

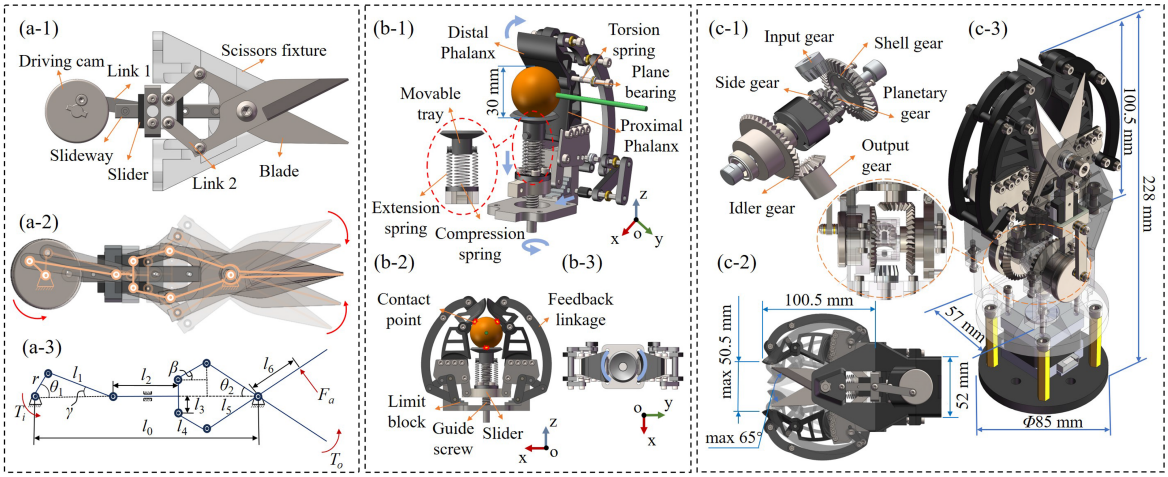

Fig. 3. (a-1) Shearing mechanism model. (a-2) Shearing motion schematic. (a-3) Kinematic model of the shearing mechanism, where r is the radius of the driving cam, l_1 is the length of the long link, l_2 is the length of the slider, l_3 is the distance of the slider mounting hole, l_4 is the length of the short link, l_5 is the length of the scissor handle, and l_6 is the contact point distance of stem, θ_1 represents the cam rotation angle, γ represents the angle between link 1 and the slider, β represents the angle between link 2 and the slider, θ_2 represents the angle between the scissor handle and the slider, T_i and T_o represent input and output torques, respectively. F_a is the shear force. (b-1) Three-dimensional flexible finger design model including the movable tray and feedback linkage. (b-2) Cross-sectional view of the concave contact surface of the finger. (b-3) Schematic of enclosed grasping, including three contact points. (c-1) Exploded view of the differential transmission mechanism. (c-2) The maximum opening angle and grasping dimensional limit. (c-3) 3D model of the gripper.

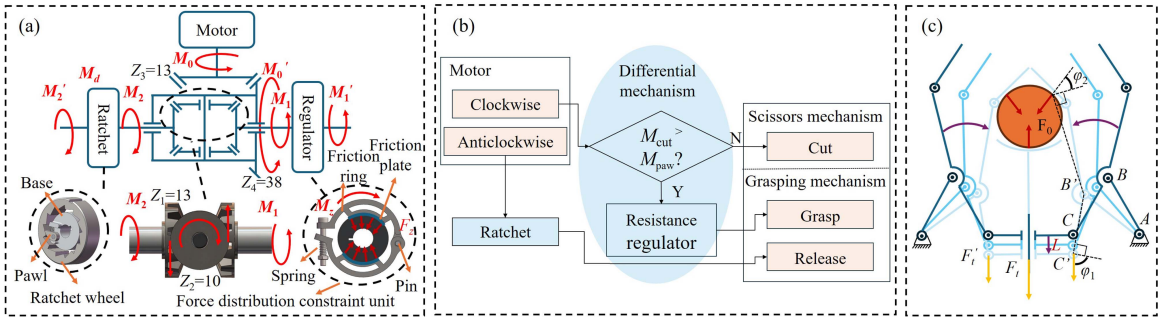

Fig. 4. (a) Auxiliary locking and grasping coupling mechanism, where: M_0 is the motor output torque, M_0' is the differential housing gear torque, M_1 and M_2 are the left and right half-axle gear torques respectively. Z_1, Z_2, Z_3 and Z_4 are the number of teeth on the side gear, planetary gear, input gear and shell gear respectively. (b) Motion strategy flowchart of the mechanism, showing how a single motor accomplishes cutting, grasping, and releasing actions. (c) Schematic diagram of finger grasping force, represented by F_0.

automatic reset. Both phalanges are injection-molded from soft polyurethane, providing cushioning during grasping. The fingertip is shaped with a front scoop to assist in clustered picking. As shown in Fig. 3(b-2), the fingers are driven by a 2 mm lead screw, ensuring precise transmission and stable grasping. A linkage system connects the distal phalanx to the limit block, suppressing lateral deformation. The limit slider provides overload protection by decoupling the grasping and shearing actions under extreme conditions. The fingers feature a curved cross section (Fig. 3(b-3)). Together, the two phalanges and a spring-loaded movable support create horizontal constraints, enabling a form-closure grasp with three contact points (Fig. 3(b-2)). This configuration enhances adaptability, reduces sensitivity to surface properties, and maintains secure grasping without continuous force, thereby minimizing fruit damage. The detailed configuration of the gear transmission is illustrated in Fig. 3(c-1). The maximum opening angle and grasping dimensional limit are shown in Fig. 3(c-2). The 3D model of the gripper is shown in Fig. 3(c-3).

D. Auxiliary Locking and Grasping Coupling Mechanism

The auxiliary locking and grasping coupling mechanism centers on a differential integrated with a ratchet and a force distribution restraint unit (Fig. 4(a)). Due to its underactuated nature, motor input follows the path of least resistance, with two output shafts driving the grasping and shearing Components. To adapt to fruits of varying stiffness, the finger grasping force is adjustable via the force distribution restraint unit, which modulates the friction. A TPE (thermoplastic elastomer) friction plate is mounted between the bossed outer surface of the bevel gear and the semicircular ring's inner surface to enhance resistance. The ring is anchored at one end by a pin and at the other with a bolt–nut–washer–spring assembly, allowing adjustment of transmission resistance by tightening the nut to increase axial force.

The ratchet mechanism ensures unidirectional shaft rotation. Clockwise rotation of the shearing mechanism shaft actuates the shearing operation to completion. Conversely, counterclockwise

rotation is resisted by the ratchet's one-way constraint, thereby channeling actuation to the grasping subsystem, as depicted in the motion-flow diagram in Fig. 4(b). The total resistance f along the gripper mechanism's transmission path can be expressed as:

$$f = f_1 + f_2 + f_3 \tag{11}$$

where f_1 denotes the resistance induced by the force distribution constraint unit, f_2 represents the applied grasping force, and f_3 corresponds to the system's intrinsic resistance.

The symmetric torque distribution across both output shafts under static loading conditions, arising from the differential's inherent mechanical equilibrium, as illustrated in Fig. 4(a).

$$M_0' = \frac{Z_4}{Z_3} M_0 \tag{12}$$

$$M_1 = M_2 = \frac{1}{2} M_0' \tag{13}$$

As shown in Fig. 4(c), the force analysis of the gripper fingers is depicted, where M_1' and M_2' represent the left and right half-axle output torques, F_t' denotes the thrust exerted by the slider on the fingers, and F_t indicates the thrust applied by the lead screw on the slider,

$$F_t' = \frac{F_t}{2} \tag{14}$$

$$M_1' = T = \frac{F_t P_h}{4\pi} \tag{15}$$

where P_h is the lead of the lead screw. The relationship between F_0 and M_1' can be derived as follows:

$$F_0 = \frac{F_t \cos\varphi_1}{\cos\varphi_2} = \frac{2\pi M_1' \varphi_1}{P_h \cos\varphi_2} \tag{16}$$

The resistance torque within a force distribution constraint unit is related to the normal pressure exerted on the friction surface, specifically:

$$M_z = \delta F_z r_z \tag{17}$$

where δ represents the coefficient of friction, F_z is the normal pressure, and r_z is the radius of the friction ring.

The resistance (M_d) offered by the ratchet mechanism is contingent upon the rotational direction of the output shaft. The resistance is negligible when rotating clockwise, but is very high when rotating counterclockwise. Eq (13) can be written as:

$$M_1' + M_z = M_d + M_2' \tag{18}$$

therefore:

$$\frac{F_0 P_h \cos\varphi_2}{2\pi\eta\cos\varphi_1} + \delta F_z r = M_d + M_2' \tag{19}$$

From (19), it can be inferred that under a constant torsional moment of the shearing mechanism, the regulator pressure (represented by F_z) exhibits a negative correlation with the grasping force (represented by F_0). Consequently, the normal load of the force distribution constraint unit can be tuned via spring compression adjustment, thus modulating finger grasping force to accommodate fruits of varying firmness. This enhances the adaptability of the gripper.

III. Experiments

A. Harvesting Strategy Verification and Experiment

A two-stage experiment was designed to evaluate the feasibility of the proposed harvesting strategy and the robustness of the customized gripper.

The objective of the first stage was to validate the effectiveness of the auxiliary locking and grasping coupling mechanism in implementing the proposed harvesting strategy. For this stage, the customized gripper was mounted on a 6-DOF robotic arm (Universal Robot 5e). A total of 30 harvesting tasks were performed on kumquats, during which the motor current was monitored in real time to track the gripper's status. Harvesting commands were sent from a host PC to an Arduino Mega 2560 controller via serial communication at a 115200 Bd rate. The controller, in turn, actuated a 42ZDT60 A motor (holding torque: 0.65 Nm; torque constant: 0.38 Nm/A) through an Emm42 V5.0 closed-loop driver.

The objective of the second stage was to evaluate the robustness of the customized gripper against dynamic disturbances. To simulate irregular wind, disturbances were introduced by randomly shaking the branches, inducing fruit oscillations of varying amplitudes. Based on the oscillation range, we defined three levels of disturbance intensity: slight ($\leq$ 2 cm), moderate ($\leq$ 5 cm), and severe ($\leq$ 8 cm). The gripper performed 30 harvesting tasks for each disturbance level. Furthermore, a conventional two-finger rigid gripper and a Fin Ray soft gripper were also tested under the same dynamic conditions, and their respective harvesting performances were recorded.

B. Resistance Adjustment and Fruit Grasping Experiment

The objective of this experiment is to validate the functional feasibility of the proposed force distribution constraint unit. Furthermore, it evaluates the gripper's capability to adapt to fruits with varying surface properties. The experiment is divided into two parts: simulated test and real test.

In the simulated harvesting test, three types of polylactic acid (PLA) models were used as target grasping objects: a 35 mm spherical model, a pear-shaped model (simulating a pear), and a textured model (simulating a strawberry). A force sensor (DS2-XD, $\pm$0.1 N) was embedded within each model. The procedure involved setting the force distribution unit to four distinct force levels by axially displacing the locknut. For each level, the gripper was actuated to perform a grasping motion on each of the three test models. Throughout this process, the maximum output grasping force applied to the target object was recorded in real-time by the embedded sensor.

In the real fruit harvesting test, a systematic experiment was conducted to evaluate the gripper's adaptability across fruits with diverse physical properties. Three representative fruits were selected to test specific capabilities: kumquats (hard stem), winter jujubes (hard fruit) and cherry tomatoes (delicate fruit). The entire process of each trial was recorded to confirm the successful completion of cutting and releasing actions. Additionally, the surfaces of all successfully harvested fruits were inspected for damage. Ultimately, the gripper's adaptability

IEEE Robotics and Automation Letters (RA-L) paper, presented at ICRA 2026, Vienna, Austria. Cite as RA-L paper.

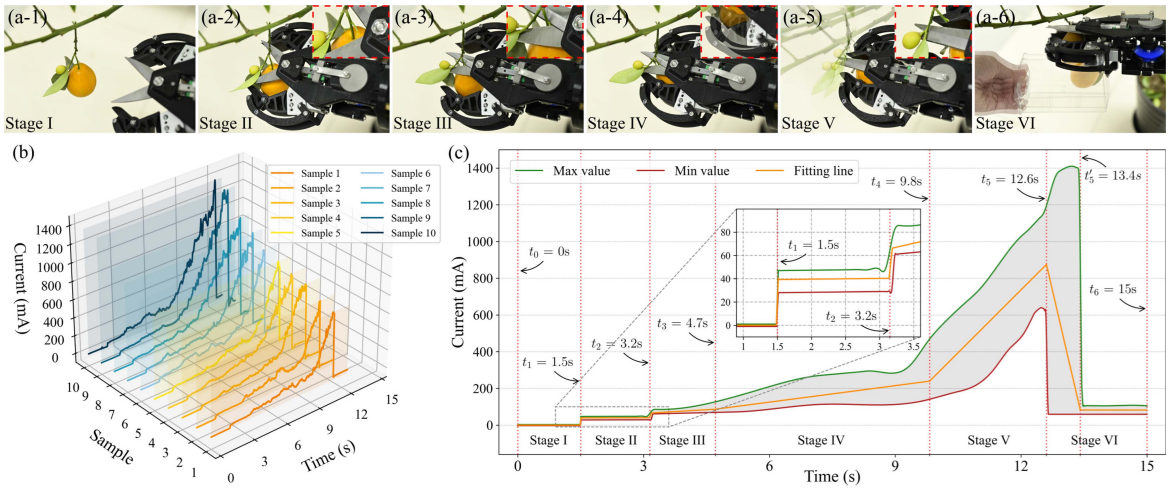

Fig. 5. Harvesting process. (a-1) State I: preparation. (a-2) State II: approaching. (a-3) State III: auxiliary fixation. (a-4) State IV: grasping. (a-5) State V: cutting. (a-6) State VI: releasing. (b) Current sampling during actual harvesting process. (c) Actual current range and fitting diagram of the harvesting process.

was comprehensively evaluated based on two key metrics: the harvesting success rate and the fruit damage rate.

IV. Results and Discussion

A. Harvesting Strategy Verification and Experiment

In the stage experiment, the gripper performed a sequence of six harvesting actions according to the predefined strategy, as illustrated in Fig. 5(a), thereby validating the effectiveness of the auxiliary locking and grasping coupling mechanism. Ten harvested samples are shown in Fig. 5(b). The motor current signal recorded during operation is presented in Fig. 5(c), with the variation pattern as follows: stage I, gripper preparation; stage II, motor activation; stage III, torque transmitted to the scissors; stage IV, torque directed to the fingers to grasp fruit by the differential, with a gradual rise in current; stage V, torque switched back to the scissors, current rapidly rising and dropping instantaneously upon cutting; stage VI, gripper release. Based on the motor torque formula Eq. (20), these current data can be used to calculate the output torque of the stepper motor.

$$\tau = AI \tag{20}$$

where I is the phase current of the motor, A is the torque constant of the motor ($A = 0.38$ Nm/A for the 42ZDT60 A). A linear model, as defined by (21), was used to fit the torque trend.

$$\tau = \begin{cases} 0.00, & t \in [0, t_1) \\ A(k_1 t + I_1), & t \in [t_1, t_2) \\ A(k_2 t + I_2), & t \in [t_2, t_3) \\ A(k_3 t + I_3), & t \in [t_3, t_4) \\ A(k_4 t + I_4), & t \in [t_4, t_5) \\ A(k_5 t + I_5), & t \in [t_5, t_6) \end{cases} \tag{21}$$

However, due to the significant current fluctuations in Phase VI, a single linear fit could not capture the trend. Therefore, this phase was modeled using a piecewise linear fit, as formulated in Eq. (22).

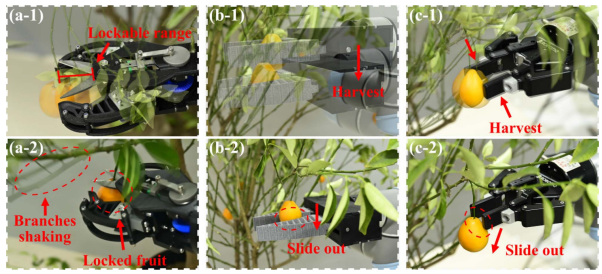

Fig. 6. Comparative experiment. (a-1) Anti-disturbance gripper preparation. (a-2) Locked fruit. (b-1) Fin-ray gripper preparation. (b-2) Slide out from Fin-ray gripper. (c-1) Two-finger gripper preparation. (c-2) Slide out from Two-finger gripper.

$$\tau = \begin{cases} A(k'_5 t + I'_5), & t \in [t_5, t'_5) \\ A(k''_5 t + I''_5), & t \in [t'_5, t_6) \end{cases} \tag{22}$$

The fitted torque curve is described by Eq. (23).

$$\tau = \begin{cases} 0.00, & t \in [0.00, 1.50) \\ 0.25t + 14.58, & t \in [1.50, 3.14) \\ 5.06t + 9.04, & t \in [3.14, 4.71) \\ 11.37t - 20.56, & t \in [4.71, 9.82) \\ 86.76t - 761.20, & t \in [9.82, 12.60) \\ -372.33t + 5045.28, & t \in [12.60, 13.41) \\ -0.10t + 32.63, & t \in [13.41, 15.00] \end{cases} \tag{23}$$

The results of the second stage experiment are depicted in Fig. 6(a). Even under intense oscillation of fruit bearing branches, the scissors of the gripper closed first, capturing and rigidly locking the swinging stem to suppress vibrations effectively. Fig. 6(b) and (c) document the typical failure modes of two commercial grippers: the Fin-Ray inspired gripper slipped due to insufficient grasping force, while the two-finger gripper failed to secure the stem owing to unstable opposition. Experimental results (Table II) indicate that the proposed gripper achieved

TABLE II
SUCCESSFULLY HARVESTING NUMBER UNDER SHAKING CONDITIONS

Shaking level	Gripper	Successes	Total	Success rate
Slight	Proposed gripper	30	30	100.0%
	Fin-ray gripper	12	30	40.0%
	Two-finger gripper	26	30	86.7%
Moderate	Proposed gripper	29	30	96.7%
	Fin-ray gripper	10	30	33.3%
	Two-finger gripper	19	30	63.3%
Severe	Proposed gripper	24	30	80.0%
	Fin-ray gripper	9	30	30.0%
	Two-finger gripper	12	30	40.0%

an 80.0% success rate under severe oscillations, and 100.0% and 96.7% under slight and moderate disturbances, respectively, outperforming both commercial designs across all disturbance levels.

The two-stage experiment substantiates the design rationale and the anti-interference advantages of the proposed gripper. The current analysis in the first stage confirmed the effective torque redistribution of the auxiliary locking and grasping coupling mechanism at different operation phases. The dynamic variation in current directly reflected the mechanical response of the system, while the fitted torque curve quantitatively characterized the force output during task execution. The second stage results further highlighted the gripper's superior performance in dynamic harvesting scenarios. When confronted with vigorously oscillating fruits, the gripper's unique locking mechanism transformed dynamic targets into quasi-static conditions, ensuring harvesting stability. In contrast, the rigid contact surfaces of the two-finger gripper often led to grasp failure or fruit damage, and the Fin-Ray inspired gripper showed limited success due to inadequate separating force. By decoupling and sequentially executing the dual tasks of stable positioning and forceful harvesting through its differential design, the proposed gripper effectively overcame the limitations of conventional designs in dynamic harvesting, thereby significantly enhancing success rates and system robustness.

B. Resistance Adjustment and Fruit Grasping Experiment

The experimental results are shown in Fig. 7. The force distribution constraint unit was successfully set to four different levels of preload. As shown in Table III, the average deviation (AD) remained below 0.2 across three model types and four preset force levels, indicating that the applied force closely matched the intended values. The average error rate (AER) remained below 4.2%. The error was smallest at high force settings and slightly higher at lower ones. Fig. 8 illustrates the six-phase harvesting sequence for three fruit types. Table IV summarizes the harvesting performance. Success rates were 86.7% for kumquats, 90.0% for winter jujubes, and 76.7% for cherry tomatoes. Winter jujubes exhibited the best performance with no observed damage, whereas kumquats had a 6.7% damage rate. Cherry tomatoes were the most vulnerable, with a 10.0% damage rate and 13.3% incomplete cuts.

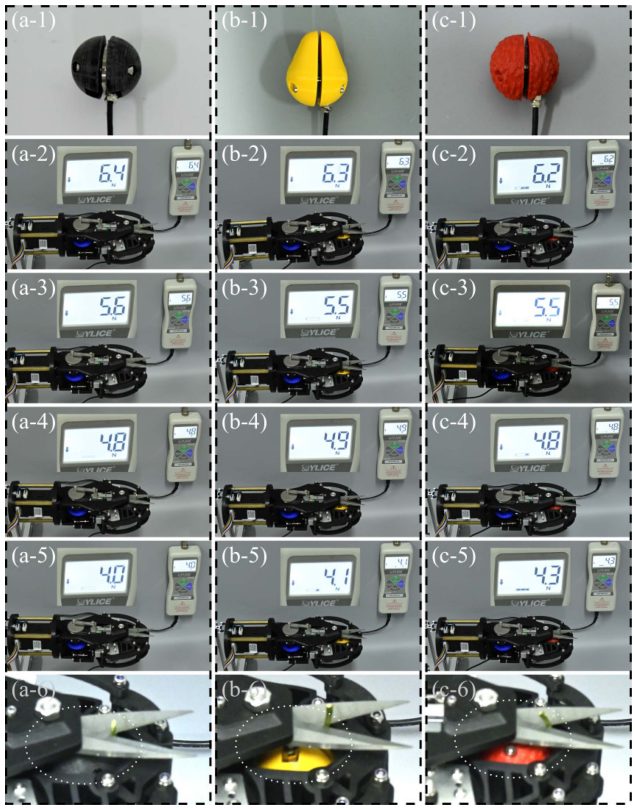

Fig. 7. Resistance adjustment experiment of (a) spherical model, (b) pear-shaped model, (c) textured model.

TABLE III
EXPERIMENTAL RESULTS OF GRASPING FORCE ADJUSTMENT

Target	SF(N)	AVG(N)	MR(N)	AD(N)	AER
Sphere	6.5	6.6	[6.3, 6.9]	0.15	2.26%
	5.5	5.5	[5.2, 5.9]	0.15	2.77%
	4.5	4.6	[4.2, 4.9]	0.17	3.98%
	4.0	4.0	[3.6, 4.4]	0.14	3.46%
Pear	6.5	6.5	[6.3, 6.9]	0.15	2.43%
	5.5	5.4	[5.1, 5.8]	0.14	2.68%
	4.5	4.6	[4.1, 5.0]	0.17	3.76%
	4.0	4.1	[3.7, 4.6]	0.17	4.15%
Texture	6.5	6.6	[6.2, 6.8]	0.17	2.48%
	5.5	5.6	[5.3, 6.0]	0.18	2.99%
	4.5	4.5	[4.2, 4.9]	0.18	3.91%
	4.0	4.1	[3.7, 4.5]	0.16	3.95%

Note: SF = Setting force, AVG = Average force, MR = Measured range, AD = Average deviation, (average absolute deviation from the arithmetic mean), AER = Average error ratio, (average percentage error between measured and set values).

TABLE IV
HARVESTING RESULTS ACROSS MULTIPLE FRUIT VARIETIES

Fruit varieties	Kumquats	Winter jujube	Cherry tomato
Success	26	27	23
Damage	2	0	3
Unsevered	2	3	4
Total	30	30	30
Success rate	86.7%	90%	76.7%

IEEE Robotics and Automation Letters (RA-L) paper, presented at ICRA 2026, Vienna, Austria. Cite as RA-L paper.

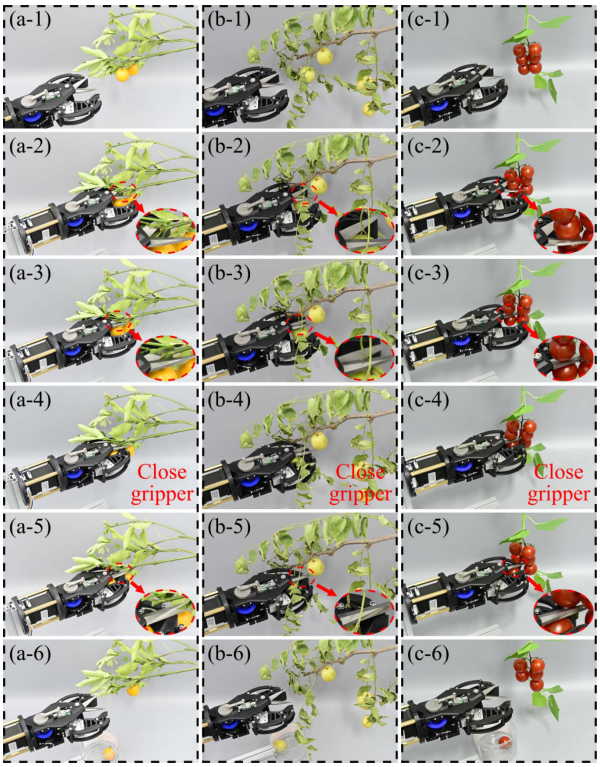

Fig. 8. Harvesting experiments of (a) kumquats, (b) winter jujube, (c) cherry tomatoes.

The experimental findings indicate that the force distribution constraint unit can effectively regulate the grasping force to harvest different fruits, with deviations maintained within acceptable limits. The slightly larger errors at low forces are mainly attributed to frictional and clearance effects, which become more pronounced in this range. In harvesting tests, the scissors mechanism exhibited high cutting efficiency, the gripper consistently generated stable grasping forces, and the force regulation strategy proved effective in protecting delicate fruits. Failures were primarily caused by positioning errors, which led to collisions with fruits or branches. Damage often occurred when the scissors inadvertently contacted the fruit during movement.

V. Conclusion

This study presents an anti-disturbance gripper for automated fruit harvesting, incorporating scissor-assisted stabilization to reduce fruit oscillations and improve grasp reliability. The modular design integrates shearing, grasping, and transmission, with a force distribution constraint unit enabling grasping force adjustment based on fruit properties to enhance adaptability and reduce damage. Maintenance is simplified, as only the friction plate or blade requires replacement with standardized parts. However, the limited grasping range of the fingers currently restricts the gripper to harvest fruits with diameters below 50 mm. Additionally, the force distribution constraint unit lacks sufficient precision for fine-tuning the grasping force. In the future, our work will focus on refining the adjustment mechanism and optimizing the finger design to accommodate a wider variety of fruit types.

References

[1] T. Wang, B. Chen, Z. Zhang, H. Li, and M. Zhang, "Applications of machine vision in agricultural robot navigation: A review," *Comput. Electron. Agriculture*, vol. 198, 2022, Art. no. 107085.
[2] R. Oberti et al., "Selective spraying of grapevines for disease control using a modular agricultural robot," *Biosyst. Eng.*, vol. 146, pp. 203–215, 2016.
[3] J. Gai, L. Tang, and B. L. Steward, "Automated crop plant detection based on the fusion of color and depth images for robotic weed control," *J. Field Robot.*, vol. 37, no. 1, pp. 35–52, 2020.
[4] J. Li et al., "Construction of a multiple-DOF under-actuated gripper with force-sensing via deep learning," *Robot.: Sci. Syst.*, 2024. [Online]. Available: https://www.roboticsproceedings.org/rss20/p101.pdf
[5] J. Li, T. Liao, H. Nigatu, H. Guo, G. Lu, and H. Dong, "Under-actuated robotic gripper with multiple grasping modes inspired by human finger," in *Proc. IEEE/RSJ Int. Conf. Intell. Robots Syst.*, 2024, pp. 5297–5302.
[6] Z. Su, Y. Ma, H. Guo, and H. Dong, "Construction of bin-picking system for logistic application: A hybrid robotic gripper and vision-based grasp planning," *IEEE Robot. Automat. Lett.*, vol. 10, no. 8, pp. 8300–8307, Aug. 2025.
[7] X. Wang, H. Kang, H. Zhou, W. Au, M. Y. Wang, and C. Chen, "Development and evaluation of a robust soft robotic gripper for apple harvesting," *Comput. Electron. Agriculture*, vol. 204, 2023, Art. no. 107552.
[8] H. Zhou, X. Wang, W. Au, H. Kang, and C. Chen, "Intelligent robots for fruit harvesting: Recent developments and future challenges," *Precis. Agriculture*, vol. 23, no. 5, pp. 1856–1907, 2022.
[9] Z. Li, X. Yuan, and C. Wang, "A review on structural development and recognition–localization methods for end-effector of fruit–vegetable picking robots," *Int. J. Adv. Robotic Syst.*, vol. 19, no. 3, 2022, Art. no. 17298806221104906.
[10] A. L. Gunderman, J. A. Collins, A. L. Myers, R. T. Threlfall, and Y. Chen, "Tendon-driven soft robotic gripper for blackberry harvesting," *IEEE Robot. Automat. Lett.*, vol. 7, no. 2, pp. 2652–2659, Apr. 2022.
[11] L. Mu, G. Cui, Y. Liu, Y. Cui, L. Fu, and Y. Gejima, "Design and simulation of an integrated end-effector for picking kiwifruit by robot," *Inf. Process. Agriculture*, vol. 7, no. 1, pp. 58–71, 2020.
[12] J. Gao et al., "Development and evaluation of a pneumatic finger-like end-effector for cherry tomato harvesting robot in greenhouse," *Comput. Electron. Agriculture*, vol. 197, 2022, Art. no. 106879.
[13] H. Dong, C.-Y. Chen, C. Qiu, C.-H. Yeow, and H. Yu, "GSG: A granary-shaped soft gripper with mechanical sensing via snap-through structure," *IEEE Robot. Automat. Lett.*, vol. 7, no. 4, pp. 9421–9428, Oct. 2022.
[14] C. W. Bac, J. Hemming, B. van Tuijl, R. Barth, E. Wais, and E. J. van Henten, "Performance evaluation of a harvesting robot for sweet pepper," *J. Field Robot.*, vol. 34, pp. 1123–1139, 2017.
[15] Y. Xiong, P. J. From, and V. Isler, "Design and evaluation of a novel cable-driven gripper with perception capabilities for strawberry picking robots," in *Proc. IEEE Int. Conf. Robot. Automat.*, 2018, pp. 7384–7391.
[16] J. Jun, J. Kim, J. Seol, J. Kim, and H. I. Son, "Towards an efficient tomato harvesting robot: 3D perception, manipulation, and end-effector," *IEEE Access*, vol. 9, pp. 17631–17640, 2021.
[17] L. Xu et al., "Design and test of end-effector for navel orange picking robot," *Trans. Chin. Soc. Agricultural Eng.*, vol. 34, no. 12, pp. 53–61, 2018.
[18] Z. Yu, J. Yuan, D. Guo, L. Du, S. Bao, and S. Ma, "Underactuated picking gripper for grasping and cutting citrus," in *Proc. IEEE Int. Conf. Robot. Biomimetics*, 2021, pp. 1935–1940.
[19] C. Lehnert, A. English, C. McCool, A. W. Tow, and T. Perez, "Autonomous sweet pepper harvesting for protected cropping systems," *IEEE Robot. Automat. Lett.*, vol. 2, no. 2, pp. 872–879, Apr. 2017.
[20] K. Motokura, M. Takahashi, M. Ewerton, and J. Peters, "Plucking motions for tea harvesting robots using probabilistic movement primitives," *IEEE Robot. Automat. Lett.*, vol. 5, no. 2, pp. 3275–3282, Apr. 2020.
[21] H. Dong, J. Zhou, C. Qiu, D. K. Prasad, and I.-M. Chen, "Robotic manipulations of cylinders and ellipsoids by ellipse detection with domain randomization," *IEEE/ASME Trans. Mechatron.*, vol. 28, no. 1, pp. 302–313, Feb. 2023.
[22] H. Yin et al., "Development, integration, and field evaluation of an autonomous citrus-harvesting robot," *J. Field Robot.*, vol. 40, no. 6, pp. 1363–1387, 2023.
[23] J. Jacob, T. Bandyopadhyay, J. Williams, P. Borges, and F. Ramos, "Learning to simulate tree-branch dynamics for manipulation," *IEEE Robot. Automat. Lett.*, vol. 9, no. 2, pp. 1748–1755, Feb. 2024.
[24] A. Rodriguez, M. T. Mason, and S. Ferry, "From caging to grasping," *Int. J. Robot. Res.*, vol. 31, pp. 886–90, 2012.